Large-area single-mode photonic bandgap vcsels

Birkedal, Dan; Gregersen, N.; Bischoff, S.; Madsen, M.; Romstad, F.; Oestergaard, J.

Published in:
Optical Fiber Communications Conference, 2003

Link to article, DOI:
10.1109/OFC.2003.1247506

Publication date:
2003

Document Version
Publisher's PDF, also known as Version of record

rate optimized e-beam generated phase shifts that result in excellent single mode yield, and a modified epitaxial structure that in the array can deliver about 50mW chip power at 300 mA drive current (at 35°C temperature).
The MEMS mirror is a double-gimbaled structure, micromachined in bulk silicon and activated electro-statically by pads underneath. The mirror itself is etched from the device layer of an SOI wafer, while the pads underneath are patterned onto a glass wafer and bonded to the SOI wafer. The mirror deflects ± 3 degrees in the horizontal direction (in the plane of the laser array) and ± 1 degree in the vertical direction at a maximum voltage of 190 volts.
There are a number of issues with this particular design that deserve further attention. Unlike the device described previously [1], the module does not monitor the fiber-coupled power directly but monitors the pointing of the MEMs mirror, thus the module is susceptible to power fluctuations caused by creep and thermal shifts. The packaging is therefore done with Au-Sn solder to minimize creep. The coupling lens is mounted on a kovar pedestal so as to move thermally with the fiber pigtail. Furthermore, the position of the beam on the quadrant detector corresponding to optimum coupling can be independently measured and stored during calibration for each laser channel so that variation of output power with the temperature of the laser assembly can be minimized. Another issue with the internal locker design is that a change in the angle of the beam reflected by the mirror will change the transmission through the etalon. If the position on the quadrant detector that corresponds to maximum fiber coupling changes from one channel to the next, the appropriate etalon signal lock point will also change. This problem is again alleviated during calibration by allowing the lock point to be stored independently for each channel.

3. Results

We have demonstrated a module capable of 20mW output power across the C-band (1529-1565nm) at a channel spacing of 25GHz. Fig. 3 shows the frequency error and the deviation of the output power from the power set point that results when the module was switched randomly among 16 channels 1000 times. Frequency accuracy of +/- 1.0GHz and power stability of +/-0.5dBm are routinely achieved. The spectral quality is similar the that of fixed wavelength DFBs, with SMSR>40dB, RIN<-140dB/Hz, and linewidth<10MHz.

[1] B. Pezeshki et al. "20mW Widely Tunable Laser Module Using DFB Array and MEMs Selection.", to appear in *IEEE Photonics Technology Letters*, September 2002.
[2] B. Pezeshki et al. "12 element multi-wavelength DFB arrays for widely tunable laser modules" in *Proc. Optical Fiber Communications Conf.*, 2002 ThGG71

MF68 **5:30 PM**

Large-Area Single-Mode Photonic Bandgap VCSELs

D. Birkedal, *Research Center COM, Lyngby, Denmark;* D. Birkedal, N. Gregersen, S. Bischoff, M. Madsen, F. Romstad, J. Oestergaard, *Alight Technologies A/S, Lyngby, Denmark, Email: Birkedal@com.dtu.dk.*

We demonstrate that the photonic bandgap effect can be used to control the modes of large area vertical cavity surface emitting lasers. We obtain more than 20 dB side mode suppression ratios in a 10-micron area device.

Introduction

Compact, efficient, and manufacturable lasers operating in the milliwatt-level output regime are increasingly in demand. Applications include, long-wavelength telecommunications, laser line-of-sight optical communications, optical storage, and high-speed laser printing. The application requires a Gaussian-type circular intensity profile that allows beam propagation over large distances, as well as focusing of high power into small spots or single-mode fibers. Vertical-cavity surface-emitting lasers (VCSELs) have attracted much attention in recent years because of their potential for high-volume low-cost manufacturability, simple two-dimensional array fabrication, and superior beam quality.
To obtain high-power operation, the active area of the device need to be increased, which increases the number of transverse modes. Combining high-power and single-mode operation is therefore a very challenging task. To solve this problem, several attempts have been put forward [1]. The most successful have used lateral modification of the effective index to create a guide or anti guide for the mode [2-4]. Others have introduced optical loss for higher order modes [5,6]. Recently a few reports have been published on a technique similar to what is used in micro structured optical fibers [7,8]. The latter technique is potentially very attractive, however, the results have so far shown low output power. The main reason for this is that the present designs have used a strong index-guide to confine the mode with a very small mode area as a result.
We show that VCSEL devices with large mode areas can be obtained using the photonic bandgap effect. Detailed calculations combining a state-of-the-art VCSEL model with an integrated photonic bandgap structure allow us to investigate the effects of thermal lensing and spatial hole burning on the performance of large area photonic bandgap VCSELs. We report on results of such modeling and first results from implementing these designs in experimental devices.

Photonic bandgap VCSEL design

To accurately design the photonic bandgap structuring of the VCSEL structure we employ a state of the art VCSEL model. The VCSEL model is based on Hadleys effective index method [9,10]. This method has been widely used in analysis of VCSEL performance. We include the effects of spatial hole burning and diffusion of carriers. In the first step we define the lateral and longitudinal

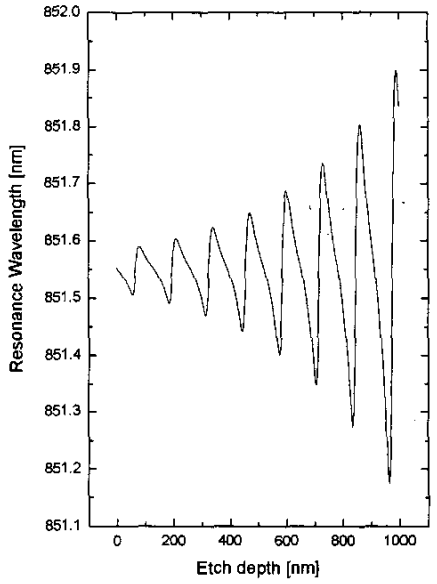

Figure 1: Cavity resonance shift as a function of surface etch depth.

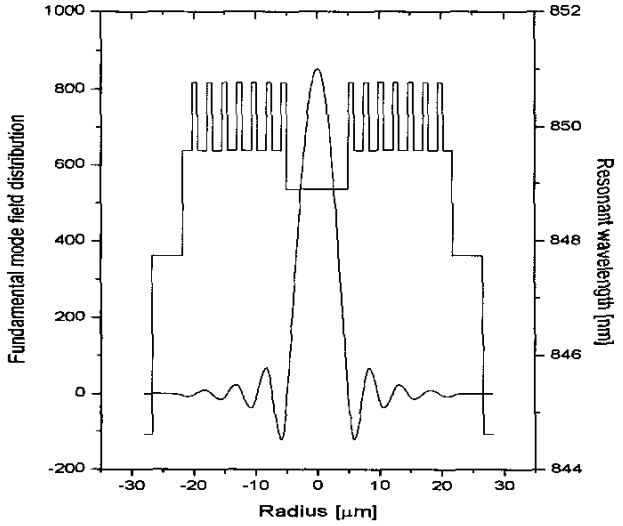

Figure 2: Real part of electrical field of the single mode confined to the defect area. Also shown is the lateral variation in the cavity resonance.

device structure. Then the spatially resolved current and temperature profiles are calculated for a given bias voltage. Using the local temperatures we adjust the refractive index and the lateral structure is sectioned into small domains of constant longitudinal index profile. The cavity resonance is then calculated for each of these lateral domains and the global lateral electromagnetic mode can be calculated. To do this we iteratively have to calculate the spatially resolved optical gain, which is a function of the local current density and optical field strength, and the local optical field strength, which is a function of the local optical gain. When the iteration is converged we can calculate the mode resolved optical power and side mode suppression ratios (SMSR). We can furthermore analyze the near field distribution of the resulting optical modes for different current injection levels.

The photonic bandgap effect is achieved by etching the top mirror of the VCSEL. Etching through the top mirror causes a change in the cavity resonance. It is the lateral modulation of the cavity resonance rather than the local effective index that enable the photonic bandgap effect. We show in Figure 1 the effect of etching through the top mirror on the cavity resonance. The modulation of the cavity resonance as a function of the etch depth reflects the periodicity of the Bragg mirror.

Results

To achieve true photonic bandgap confinement of the lasing mode we design a structure where a lateral mode is confined to a defect region and prohibited from propagating in a photonic bandgap region due to multiple reflections. We show in Figure 2 the lateral cavity resonance modulation in a structure with a defect of 10-micron diameter. The structure confines a single transversal mode to the defect as shown in Figure 2. In an oxide confined VCSEL with a 10-micron aperture there would typically be 30 – 40 confined in the cold cavity.

As the injection current is increased heating causes a thermal lens to form in the defect region. This thermal lens is responsible for a second mode to be confined by the photonic bandgap regions. This causes the laser to operate on several transversal modes. To illustrate this we calculate the light-current characteristics for the device as shown in Figure 3. The Figure shows the total output power and the power in the four most intense modes. The laser turns on in a single transversal mode at 5 mA and remains single moded up to a current of 12 mA. This is reflected in the SMSR, which we show in Figure 4. We see that the laser has a SMSR of more than 20 dB in the injection current range from 5 mA – 12 mA. We note that the present structure has not yet been optimized with respect to single-mode output-power. We expect to achieve considerably higher single-mode output-power levels in an optimized structure.

One of the advantages of this structure is that the mode profile is relatively insensitive to the current injection level. To illustrate this feature we plot in Figure 5 the radial intensity profile for three different injection levels: near threshold, intermediate, and just before onset of multi-mode operation. In the present case the half width of the intensity profile changes less than a few %, which is considerably better, than for oxide confined VCSELs. The stability of the mode profile to current and hence temperature is important for efficient coupling to single mode fibers.

Conclusions

We have demonstrated that large-area single-mode VCSELs can made using the photonic bandgap effect. These lasers have potential to reach multi milliwatt in a single transversal mode, which enable a range of new application for VCSELs. We have furthermore demonstrated the stability of the single transversal mode for increasing injection current. We are currently implementing the present design and well show first experimental results.

References

1. For a recent review see: J.-F.P. Seurin, S.L. Chuang, L.M.F. Chirovsky, and K.D. Choquette, "Novel VCSEL designs deliver high single-mode output power", Laser Focus World, pp. 119–122,

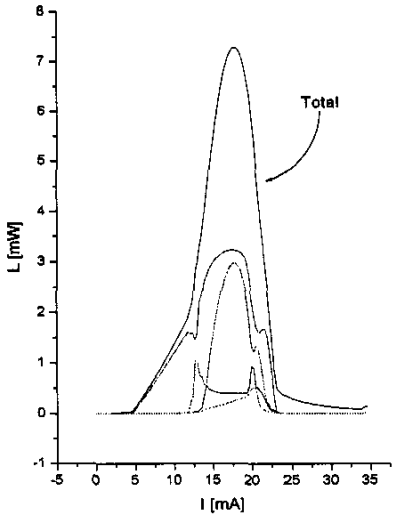

Figure 3: Light current characteristics. The total output power and the power in the four most intense modes are plotted against the injection current.

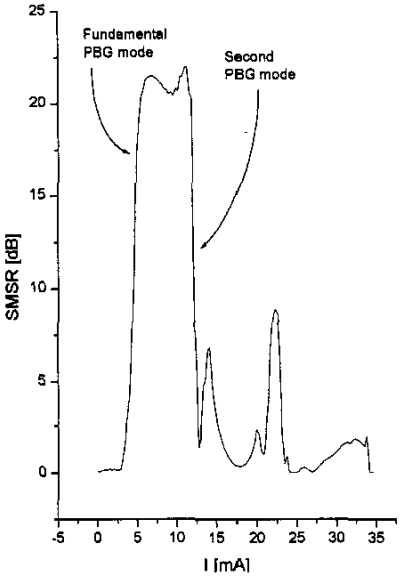

Figure 4: Side mode suppression ratio (SMSR) plotted against the injection current. The figure shows the onset of lasing on the second confined photonic bandgap mode.

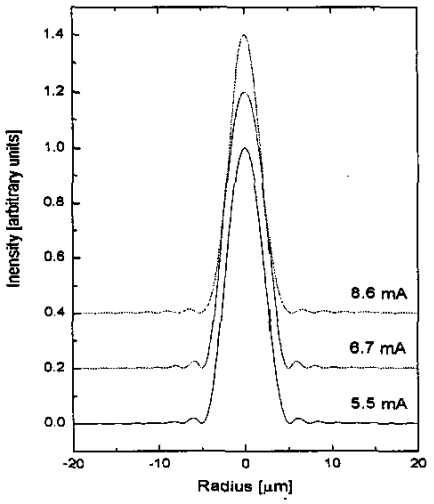

Figure 5: Near field profiles of the lasing mode. The figure shows profiles of the optical intensity at the laser facet for three different current injection levels.

May, 2002.
2. B. J. Koch, J. R. Leger, A. Gopinath, Z. Wang, and R. A. Morgan, "Single-mode vertical cavity surface emitting laser by graded-index lens spatial filtering," Appl. Phys. Lett., vol. 70, pp. 2359–2361, 1997.
3. Y. A. Wu, C. J. Chang-Hasnain, and R. Nabiev, "Single mode emission from a passive-antiguide-region vertical-cavity surface-emitting laser," Electron. Lett., vol. 29, pp. 1861–1863, 1993.
4. T.-H. Oh, M. R. McDaniel, D. L. Huffaker, and D. G. Deppe, "Cavity-induced antiguiding in a selectively oxidized vertical-cavity surface-emitting laser," IEEE Photon. Technol. Lett., vol. 10, pp. 12–14, Jan. 1998.
5. H. Martinsson, J. A. Vuku˘sic´, and A. Larsson, "Single-Mode Power Dependence on Surface Relief Size for Mode-Stabilized Oxide-Confined Vertical-Cavity Surface-Emitting Lasers," IEEE Photon. Technol. Lett., vol. 12, pp. 1129–1131, 2000.
6. H.J. Unold, M. Golling, F. Mederer, R. Michalzik, D. Supper, and K.J. Ebeling, "Singlemode output power enhancement of InGaAs VCSELs by reduced spatial hole burning via surface etching," Electron. Lett., vol. 37, pp. 570–571, 2001.
7. ECOC: H.J. Unold, M. Golling, R. Michalzik, D. Supper, and K.J. Ebeling, "Photonic crystal surface-emitting lasers: tailoring waveguiding for single-mode emission," ECOC 2001 Amsterdam, The Netherlands.
8. D.–S. Song, S.-H. Kim, H.-G. Park, C.-K. Kim, and Y.-H. Lee, "Single-fundamental-mode photonic-crystal vertical-cavity surface-emitting lasers," Appl. Phys. Lett., vol. 80, pp. 3901-3903, 2002.
9. G.R. Hadley, "Effective index model for vertical-cavity surface-emitting lasers," Opt. Lett., vol. 20, pp. 1483-1485, 1995.
10. J.A. Vukusic, H. Martinsson, J.S. Gustavsson, and A. Larsson, "Numerical Optimization of the Single Fundamental Mode Output from a Surface Modified Vertical-Cavity Surface-Emitting Laser," IEEE J. Quant. Elec., vol. 37, pp. 108-117, 2001.

MF69 **5:30 PM**

High Power C-Band Semiconductor Booster Optical Amplifier

M. Dagenais, P. Heim, S. Saini, S. Wilson, R. Leavitt, A. Yu, T. Horton, V. Luciani, D. Stone, Y. Hu, *Quantum Photonics Inc, Jessup, MD, Email: dagenais@quantumphotonics.com.*

A semiconductor booster optical amplifier chip with a saturation power of 20.2 dBm has been demonstrated to operate over the whole C-band. This booster amplifier was used in 10 Gb/s propagation experiment over 80 km of single mode fiber

Introduction

As the complexity and functionality of WDM systems increases, the need for optical amplification also increases. Until now this need has been fulfilled, to a large extent, by erbium doped fiber amplifiers (EDFAs). So far, optical amplification has been used in booster and in-line applications, as loss compensators for chromatic and dispersion compensators, and also as pre-amplifiers for high sensitivity detection. Upcoming applications include reconfigurable add-drop multiplexers and dynamic gain equalization. Recently, we have seen tremendous pressure toward reducing the cost of optical components. Lower cost optical amplifiers have appeared on the market. These include erbium doped waveguide amplifiers (EDWAs) and semiconductor optical amplifiers (SOAs). SOAs have found uses in booster applications for boosting the power of fixed frequency and tunable semiconductor lasers (i.e. tunable VCSELs) and as in-line amplifiers. For these applications, high saturation power over the whole C-band and low noise-figure to preserve signal quality of the incident beam are required. Recently, high saturation power SOAs have been discussed [1,2]. Here, we report on an ultra-high

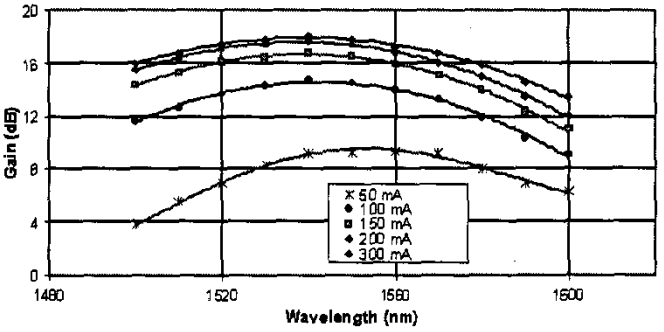

Figure 1. Gain spectra as function of bias current

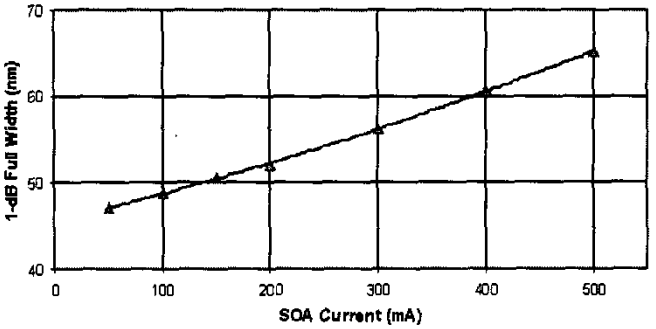

Figure 2. Gain Bandwidth versus bias current

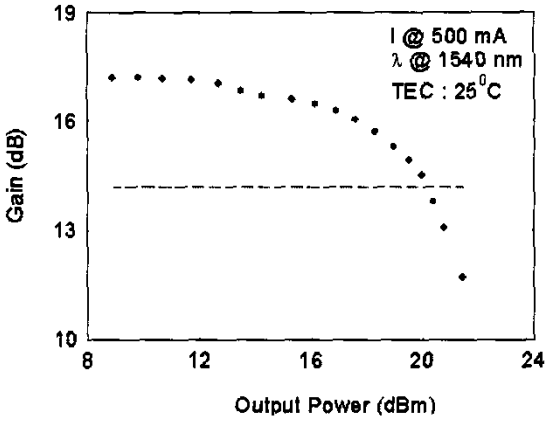

Figure 3. Gain saturation versus output optical power

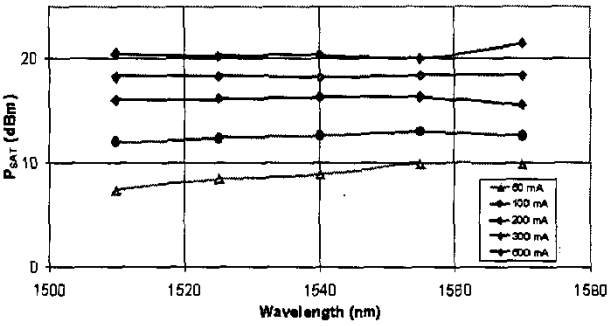

Figure 4. Dependence of Psat on wavelength at different currents